The EMBO Journal vol.12 no.1 pp.1-8, 1993

Electron diffraction analysis of structural changes in the photocycle of bacteriorhodopsin

Sriram Subramaniam[1,2], Mark Gerstein[1], Dieter Oesterhelt[3] and Richard Henderson[1]

[1]MRC Laboratory of Molecular Biology, Hills Road, Cambridge CB2 2QH, UK, [2]Department of Biological Chemistry, Johns Hopkins University School of Medicine, Baltimore, MD 21205, USA and [3]Max-Planck Institut für Biochemie, D-8033, Martinsried, Germany

Communicated by R.Henderson

Structural changes are central to the mechanism of light-driven proton transport by bacteriorhodopsin, a seven-helix membrane protein. The main intermediate formed upon light absorption is M, which occurs between the proton release and uptake steps of the photocycle. To investigate the structure of the M intermediate, we have carried out electron diffraction studies with two-dimensional crystals of wild-type bacteriorhodopsin and the Asp96→Gly mutant. The M intermediate was trapped by rapidly freezing the crystals in liquid ethane following illumination with a xenon flash lamp at 5 and 25°C. Here, we present 3.5 Å resolution Fourier projection maps of the differences between the M intermediate and the ground state of bacteriorhodopsin. The most prominent structural changes are observed in the vicinity of helices F and G and are localized to the cytoplasmic half of the membrane.

Key words: conformational change/M-intermediate/retinal proteins/seven-helix receptors/signal transduction

Introduction

Bacteriorhodopsin is a light-driven proton pump found in *Halobacterium halobium* (Stoeckenius *et al.*, 1979; Khorana, 1988; Oesterhelt *et al.*, 1991). The mechanism of proton translocation is now understood to involve the following steps: (i) isomerization of retinal from the *all-trans* to the 13-*cis* configuration, (ii) transfer of a proton from the protonated Schiff base to the deprotonated carboxylate of Asp85, (iii) release of a proton into the extracellular medium from an as yet undetermined group, (iv) transfer of a proton from the protonated carboxylate of Asp96 to the Schiff base, (v) uptake of a proton from the cytoplasmic medium and, finally, (vi) protein-driven reisomerization of retinal from the 13-*cis* to the *all-trans* configuration. The specific sequence of these steps is variable depending on the pH and ionic strength of the medium [see *J. Bioenerget. Biomembr.*, **24**(2) (1992) for recent reviews on functional studies with bacteriorhodopsin]. The cycle of proton transport is accompanied by changes in the absorption spectrum of the retinylidene chromophore which correspond to the formation and decay of at least five distinct intermediates (Lozier *et al.*, 1975). The main intermediates of the photocycle and their relation to the release and uptake of protons are presented in Figure 1.

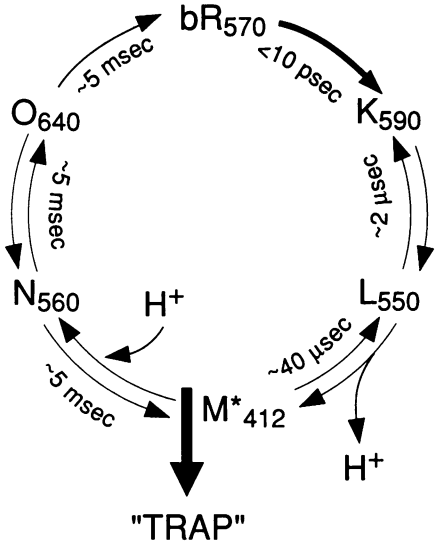

Fig. 1. The photocycle of bacteriorhodopsin at 25°C. The kinetic scheme is that described in Lozier *et al.* (1975) except for the inclusion of back reactions. The steps during which the Schiff base releases and takes up a proton are indicated. Although a single M intermediate is shown, it is believed that there are at least two distinct forms: M1, where the Schiff base is accessible to the extracellular side, and M2, where the Schiff base is accessible to the cytoplasm (Varo and Lanyi, 1991). The bold vertical arrow shows the stage of the photocycle at which the samples are plunged into liquid ethane.

Henderson *et al.* (1990) have reported a structure for bacteriorhodopsin based on high resolution electron cryo-microscopy. This model provides a structural context for the main features of the pathway of proton translocation, proposed from biochemical, spectroscopic and mutagenesis experiments. To understand fully the chemical mechanism of light transduction by bacteriorhodopsin, it is necessary to determine the changes in protein structure at specific steps in the photocycle. Here, we report 3.5 Å resolution projection maps of the conformational changes associated with the formation of the M intermediate in the bacteriorhodopsin photocycle.

In an earlier effort to determine the structure of the M intermediate using electron diffraction of dried, glucose-embedded specimens of bacteriorhodopsin, Glaeser *et al.* (1986) did not observe any major structural changes upon light absorption. This observation disagrees with recent neutron and X-ray diffraction analyses of the photocycle using fully hydrated membrane samples (Dencher *et al.*, 1989; Koch *et al.*, 1991; Nakasako *et al.*, 1991) which showed large structural changes. The source of the conflict between these observations could be that the exchange of structurally important water molecules with glucose prevented the occurrence of light-induced conformational changes. The experiments reported here have been carried out using fully hydrated specimens (see Figure 2 and

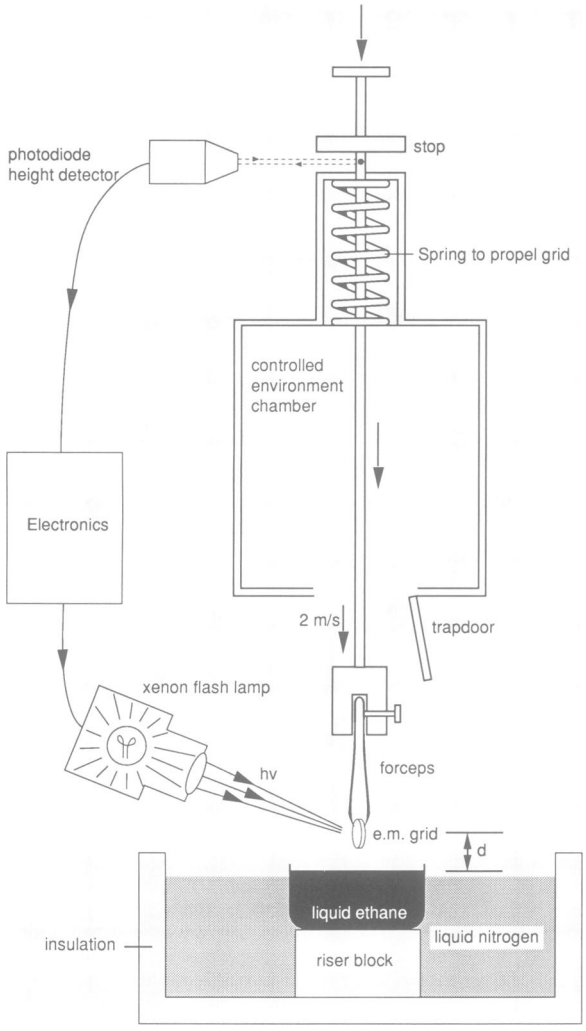

Fig. 2. Schematic diagram of the apparatus to trap photointermediates (also see text in Materials and methods). A double action cable release is used to simultaneously open the trap door and propel the plunger with the clamped grid into liquid ethane. The flash lamp is triggered to deliver a focused beam to the grid when it is at a defined distance, 'd', above the surface of the liquid ethane using photodiode activated electronics. Since the speed of the plunger is ~2 m/sec, illumination of the grid 4 cm above the liquid ethane surface gives a delay of ~20 ms before the grid is frozen.

description in Materials and methods) to avoid any artefacts due to embedding in glucose. Although the X-ray and neutron diffraction experiments were carried out at much lower resolution and with fewer Fourier terms, we find that they are in close agreement with the present electron diffraction analysis. The location of the structural changes in the protein provides important clues to the mechanism of proton transport by bacteriorhodopsin.

Rationale and design of experiment to trap photointermediates

To trap the M intermediate within its lifetime, we have made use of spectroscopic studies that provide quantitative information on the composition of photointermediates at various times after illumination of bacteriorhodopsin. Replacement of Asp96 by Gly, Ala or Asn prolongs the lifetime of the M intermediate by about two orders of magnitude compared with wild-type bacteriorhodopsin (Marinetti *et al.*, 1989; Tittor *et al.*, 1989; Otto *et al.*, 1990). This effect is due to the absence of the carboxylate at residue 96, which is protonated in the ground state and functions as an internal proton donor to the Schiff base during the M→N step of the photocycle. We chose the mutant with the Gly substitution because the difference in size between Asp and Gly residues could be used to determine the location of the Asp96 side chain.

At 25°C, the photocycle of wild-type bacteriorhodopsin is essentially complete within 20 ms (Lozier *et al.*, 1975). In contrast, in the Asp96→Gly (D96G) mutant, the decay of the M intermediate is ~100-fold slower than the wild-type photocycle (Tittor *et al.*, 1989). Thus, 20 ms after illumination at 25°C, the majority of the molecules of the D96G mutant remain in the M stage of the photocycle, whereas most of the molecules in the wild-type crystal have returned to the ground state.

The kinetics of the photocycle display a sharp temperature dependence, and the cycling time is lengthened ~10-fold as the temperature is lowered from 25°C to 5°C (Varo and Lanyi, 1991). Thus, at 5°C, a considerable amount of the M intermediate is present in wild-type bacteriorhodopsin even 20 ms after illumination. The main difference between the wild-type and the mutant is that in wild-type bacteriorhodopsin, measurable amounts of the N and O intermediates are also present along with M. To determine the structural changes during the photocycle of both wild-type bacteriorhodopsin and the D96G mutant, we have collected diffraction patterns from four sets of specimens: (i) D96G mutant trapped 20 ms after illumination at 25°C (composition ~92% M, ~8% bacteriorhodopsin; Tittor *et al.*, 1989); (ii) wild-type bacteriorhodopsin trapped 20 ms after illumination at 25°C (composition <1% N, <1% O, >98% bacteriorhodopsin; Varo and Lanyi, 1991); (iii) wild-type bacteriorhodopsin trapped 10 ms after illumination at 5°C (composition ~63% M, ~26% N, ~3% O, ~8%

Fig. 3. Two-dimensional projection Fourier maps. The solid triangles in each map indicate the locations of the three-fold axes, and the grid bars are spaced at 21 Å, which is one-third of the unit cell. (**a**) Wild-type bacteriorhodopsin at 3.5 Å resolution. The seven helices are identified. For helices that are significantly tilted with respect to the membrane normal, the top and bottom ends are indicated. Thus, A, E, F and G mark the locations of the cytoplasmic ends of these helices, whereas A′, E′, F′ and G′ mark the respective extracellular ends. (**b**) Difference map between the D96G mutant and wild-type bacteriorhodopsin, obtained from averaging two separate difference maps: (i) difference in diffraction patterns obtained from seven glucose-embedded crystals of the D96G mutant and the wild-type reference data set reported in Ceska and Henderson (1990), (ii) difference between diffraction patterns from 12 crystals of the D96G mutant and 17 crystals of wild-type bacteriorhodopsin, both under fully hydrated conditions. The Asp96 side chain is marked. (**c**) Difference map of structural changes in the D96G mutant 20 ms after illumination at 25°C, pH 8.5, obtained using eight illuminated and 12 unilluminated crystals. (**d**) Difference map of structural changes in wild-type bacteriorhodopsin 10 ms after illumination at 25°C, pH 8.5, obtained using three illuminated and three unilluminated crystals. (**e**) Difference map of structural changes in wild-type bacteriorhodopsin 20 ms after illumination at 5°C, pH 7.0, obtained using eight illuminated and nine unilluminated crystals. (**f**) Difference map of structural changes in wild-type bacteriorhodopsin 20 ms after illumination at 5°C, pH 7.0, obtained using seven illuminated and nine unilluminated crystals. The solid lines seen in all the maps have been drawn to show the approximate boundaries of individual molecules in the trimer. All difference maps (b–f) have been contoured at the same interval, which, in turn, is eight times smaller than the contour interval used for the projection map shown in panel a.

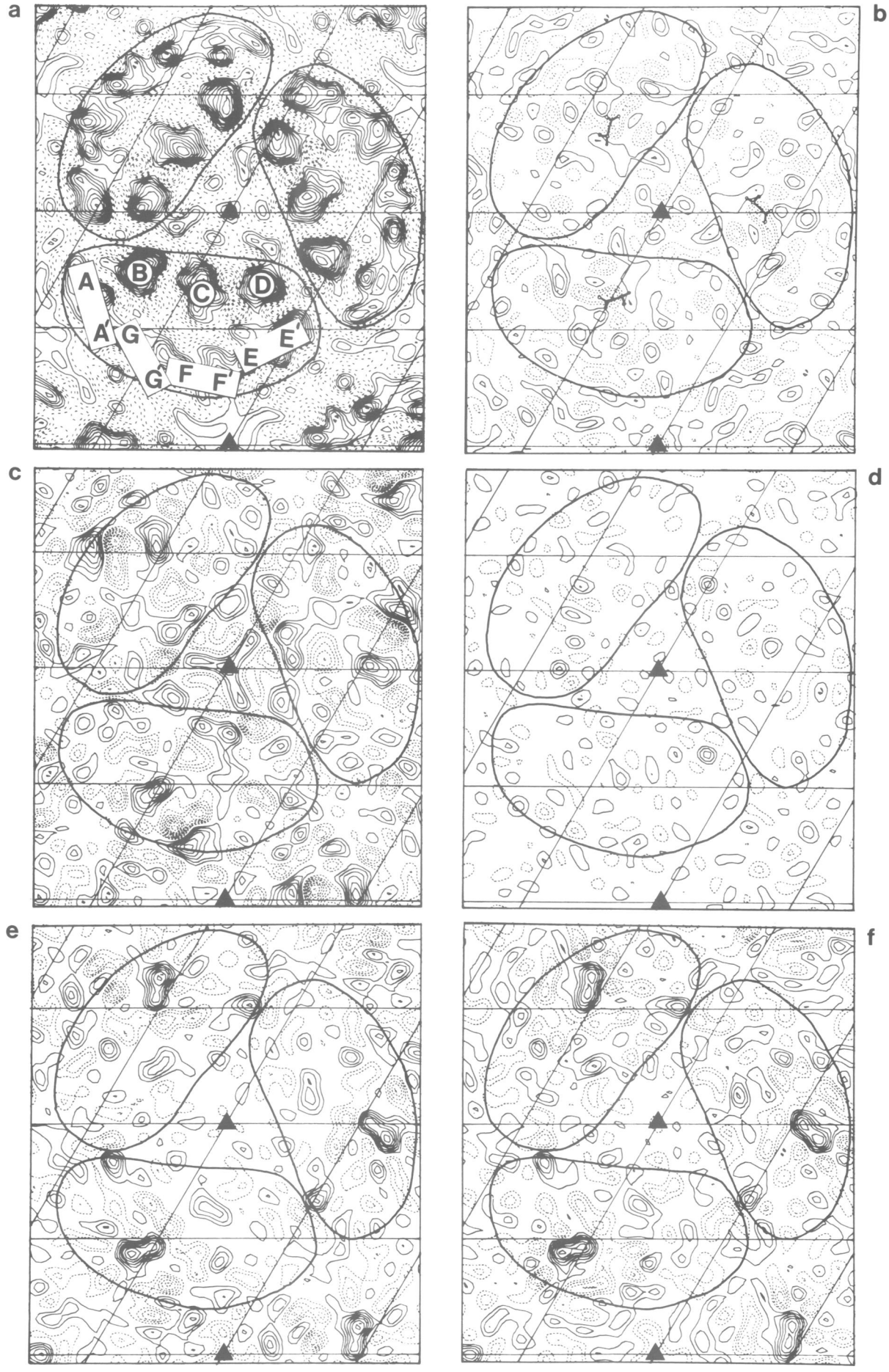
a
b
c
d
e
f
A
B
C
D
A'
G
E'
G'
F
F'
E

bacteriorhodopsin; Varo and Lanyi, 1991); (iv) wild-type bacteriorhodopsin trapped 20 ms after illumination at 5°C (composition ~48% M, ~27% N, ~4% O, ~21% bacteriorhodopsin; Varo and Lanyi, 1991).

In all cases, diffraction patterns were also recorded from crystals frozen under identical conditions in the absence of illumination. Overall, our expectation was that the (light−dark) difference Fourier maps from the D96G mutant at 25°C and wild-type bacteriorhodopsin at 5°C would display comparable features, with any differences possibly reflecting the variations in the composition of the photointermediates.

Results

Difference map between wild-type bacteriorhodopsin and the D96G mutant in the absence of illumination

Crystals of both wild-type bacteriorhodopsin and the D96G mutant diffracted to a resolution of better than 3.5 Å. The diffraction patterns were processed as described in Materials and methods, and the averaged intensities from reflections with z* values ranging from −0.007 to +0.007 $Å^{-1}$ were then used to construct difference Fourier maps in projection. In Figure 3a, a Fourier map of native bacteriorhodopsin at a resolution of 3.5 Å is shown. Figure 3b shows the difference map between the D96G mutant and wild-type bacteriorhodopsin obtained as explained in the figure legend. Although the map has a poor signal/noise ratio, the largest peak in the map is negative and is within 1 Å of the position of the Asp96 carboxylate in the structural model for bacteriorhodopsin (Henderson *et al.*, 1990). This result indicates that the structures of the D96G mutant and wild-type bacteriorhodopsin are nearly the same in the ground state.

Projection map of structural changes in wild-type bacteriorhodopsin and the D96G mutant at 25°C

For both wild-type bacteriorhodopsin and the mutant, no difference in resolution was observed between diffraction patterns collected in the absence and presence of illumination. This establishes that conversion of the sample to the M or N intermediates does not alter its crystallinity. The maps shown in Figure 3c−f are computed from differences in diffraction intensities observed between illuminated and non-illuminated grids of a particular type of specimen, using phases from native bacteriorhodopsin. Figure 3c shows a difference map obtained from the D96G mutant, frozen 20 ms after illumination at 25°C, pH 8.5. The most prominent peaks in the map are near helices F and G. A large increase in density is observed nearest to helix G along with a distribution of negative peaks in the surrounding region. The pair of closely apposed negative and positive peaks localized on helix F suggest a net outward movement of helix F away from the central portion of the protein. A set of smaller displacements are also observed in the vicinity of helices C, D and E. It is apparent that there are more changes on the region of the molecule covered by helices C, D, E, F and G than there are on the region of the molecule covered by helices A and B.

The control experiment with wild-type bacteriorhodopsin comparing illuminated and non-illuminated samples at 25°C is shown in Figure 3d. As discussed in the previous section, the wild-type photocycle is almost complete at 20 ms after illumination at 25°C. As expected, no substantial differences are seen. The map shows a random distribution of positive and negative peaks and provides a measure of the noise level in the difference Fourier maps presented here. Note that the features in all the other difference maps, including Figure 3b, have many more contours. For another independent measure of the noise level, 12 diffraction patterns from unilluminated D96G crystals were randomly divided into two sets of six. The difference projection map constructed by comparing these two sets had the same noise level as the map shown in Figure 3d (data not shown).

Projection map of structural changes in wild-type bacteriorhodopsin at 5°C

Figure 3e shows a projection map of the structural changes in wild-type bacteriorhodopsin 10 ms after illumination at 5°C, pH 7.0. Under these conditions both the M and N intermediates are present. The changes in density that are observed here are similar but not identical to those found for the M intermediate obtained with D96G (Figure 3c). The main features here are a large positive peak centred on helix G and an apparent movement in the vicinity of helix B, as indicated by adjacent positive and negative peaks. Significantly, the density changes seen near helices C, D and E in the difference map of Figure 3c are absent in Figure 3e. Thus, the structural changes appear to be localized to the region of the molecule covered by helices A, B and G rather than to the region covered by helices C, D, E and F.

The difference Fourier map from wild-type bacteriorhodopsin frozen 20 ms after illumination at 5°C is shown in Figure 3f, and is very similar to the map shown in Figure 3e. The similarities between the difference maps obtained 10 and 20 ms after illumination is consistent with the similar compositions of the photointermediates at these times, and is a further indication of the levels of reproducibility and noise in our analysis. Similar structural changes were observed when the M intermediate was trapped at pH 5.5 and at pH 8.5.

Location of structural changes in the third dimension

Although the projection maps shown in Figure 3 are at a resolution of 3.5 Å in the plane of the membrane, they provide no information on the vertical location of the structural changes in the protein. Using diffraction patterns obtained from grids tilted up to 10°, we have constructed a preliminary three-dimensional map to determine whether the structural changes in the vicinity of helices F and G are localized to the cytoplasmic or the extracellular half of the protein (Figure 4). Despite the limited 50 Å vertical resolution, the principal features seen in the projection maps (Figure 3 panels c, e, f and Figure 4a) are localized to the cytoplasmic half (+20 Å section). We hope to collect more diffraction patterns with higher tilts to improve the resolution of the measurement in the vertical direction.

Discussion

Correlation of the present electron diffraction analysis with previous structural studies on the M intermediate

It is instructive to compare the present electron diffraction analysis with earlier efforts to study the structure of the M intermediate. Frankel and Forsyth (1985) reported that formation of the M intermediate results in a loss of order

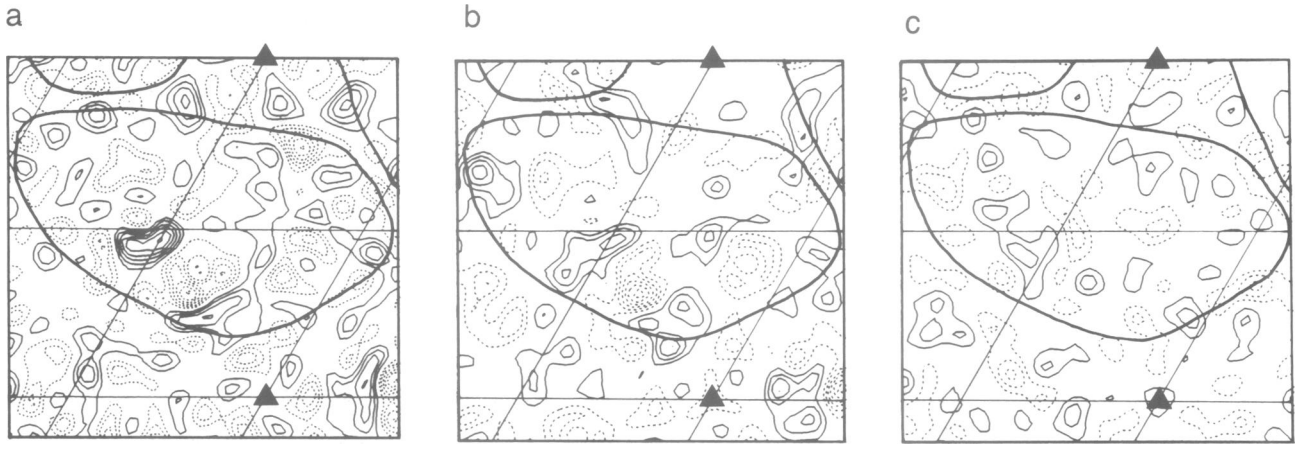

Fig. 4. Difference Fourier maps calculated using a total of 35 electron diffraction patterns from illuminated membranes (14 D96G mutant, 21 wild-type) and 28 patterns from unilluminated membranes (15 D96G mutant, 13 wild-type) which were tilted at angles distributed over the range ±10°. The data are a combination of patterns from the D96G mutant and wild-type bacteriorhodopsin, merged into one 'mixed' three-dimensional data set to produce lattice line curves (Ceska and Henderson, 1990; Glaeser *et al.*, 1986) extending to limited z* values of ±1/50 Å^{-1}. The choice of contour levels is arbitrary. (**a**) Projection map calculated using only z* = 0.0 Å^{-1} data from the curves. The features here are an average of those seen in Figure 3 panels c, e and f. (**b**) Section of three-dimensional map at height +20 Å from retinal showing difference density in the cytoplasmic half. (**c**) Section of three-dimensional map at height −20 Å from retinal showing difference density in the extracellular half. The noise level and vertical resolution in (b) and (c) are rather poor because the amount of data is still limited.

in two-dimensional crystals. This finding has not been substantiated in any of the subsequent studies, including our present experiments. Based on electron diffraction studies, Glaeser *et al.* (1986) reported that essentially no protein structural changes occurred upon formation of a yellow intermediate, presumed to be the same as the M intermediate. This work was carried out using dried, glucose-embedded purple membranes, with a yellow intermediate trapped by continuous illumination of a slowly cooled specimen. More recently, three independent efforts have been made to address the problem of the structure of M. (i) Low temperature neutron diffraction experiments carried out on wild-type bacteriorhodopsin in the presence of guanidine at alkaline pH (Dencher *et al.*, 1989), (ii) time-resolved X-ray experiments carried out on the D96N mutant and wild-type bacteriorhodopsin soaked in guanidine at alkaline pH (Koch *et al.*, 1991) and (iii) time-resolved X-ray experiments carried out on wild-type bacteriorhodopsin soaked in an arginine buffer at alkaline pH (Nakasako *et al.*, 1991). The latter three studies were carried out on multilayer stacks of hydrated bacteriorhodopsin-containing membranes; the results indicated that there were significant changes in the tertiary structure of bacteriorhodopsin during the photocycle. The present electron diffraction experiments support the observations from the X-ray and neutron diffraction experiments. For purposes of comparison, we note that the difference maps presented here were derived from 143 non-overlapping Fourier terms to 3.5 Å resolution, whereas the X-ray and neutron analyses were based on ~20 observations to 7 Å resolution. Furthermore, most of the measurements made in the neutron and X-ray work represent unresolved pairs of overlapping reflections, in which the relative contribution of each member of the pair to the difference coefficients is unknown.

Table I gives the variation in diffraction patterns from selected illuminated crystals when compared against the average from the eight illuminated crystals used to construct the map in Figure 3c. For each diffraction pattern, two parameters were calculated: (i) the correlation in the amplitude change of individual reflections and (ii) the extent of photoconversion to the M intermediate, measured by comparing the magnitude and change in amplitude of all common reflections (see Materials and methods for further details). The diffraction patterns obtained from unilluminated crystals (E233, E380, F341 and F764) show no correlation with the light-induced structural changes. The range of these values for illuminated samples (D290, E848, F333 and F741) indicates that the intrinsic variation in sample illumination between different experiments is about ±20%. The entries for crystals E380 and F764 represent the largest sample-to-sample variation observed in the experiments.

Table I. Quantitative comparison of amplitude changes in selected single crystals with the averaged data set used to construct the difference Fourier map in Figure 3c

Crystal number	Remarks	Correlation coefficient[a]	Extent of change[a]
D290	mutant, illuminated	0.87	1.17
E848	mutant, illuminated	0.72	1.21
F333	wild-type, illuminated	0.66	1.17
F741	wild-type, illuminated	0.48	0.80
E233	mutant, dark	−0.06	−0.15
E380	mutant, dark	−0.14	−0.28
F341	wild-type, dark	0.01	−0.03
F764	wild-type, dark	0.03	0.27

[a]Correlation coefficient and extent of change calculated as described in Materials and methods. The values of ΔF1 are the differences between the eight illuminated and 12 unilluminated crystals used in Figure 3c. The values of ΔF2 are differences between the individual film and the same 12 unilluminated samples.

Table II presents pairwise comparisons of the X-ray and electron diffraction analyses of the M intermediate, calculated as above, but using the intensity changes in reflections that are common to both experiments. The correlation of the two independent X-ray analyses (0.70) is comparable to the individual correlation of each with the present electron diffraction analysis (0.67 and 0.57). This agreement is excellent given the different scattering cross-sections of X-

Table II. Quantitative comparison of changes observed in present electron diffraction work with the changes observed in previous electron diffraction amplitudes and X-ray diffraction intensities

Data set #1	Data set #2	Correlation coefficient[a]	Ratio of intensity change[a] in data set # 1 compared with data set # 2
Koch *et al.* (1991)	Nakasako *et al.* (1991)	0.70	1.31[b]
Nakasako *et al.* (1991)	Koch *et al.* (1991)	0.70	0.76[b]
Glaeser *et al.* (1986)	Nakasako *et al.* (1991)	0.12	0.08
Glaeser *et al.* (1986)	Koch *et al.* (1991)	0.10	−0.14
Glaeser *et al.* (1986)	data in Figure 3c	−0.17	−0.13
Koch *et al.* (1991)	data in Figure 3c	0.67	1.23
Nakasako *et al.* (1991)	data in Figure 3c	0.57	0.63

[a]Correlation coefficient and extent of change calculated as described in Materials and methods.
[b]Since the formula for the extent of change depends on which data set is used as the reference, these two values are not exact reciprocals of each other.

rays and electrons. The electron diffraction data reported in Glaeser *et al.* (1986) show no correlation with either the X-ray diffraction experiments or the present electron diffraction work. Hence, the structural changes observed in our work are similar to the changes observed in the X-ray work, but not to the previous electron diffraction work using glucose-embedded specimens.

In our experiments, we have not been able to measure an absorption spectrum of the adsorbed crystals, since a complete monolayer of bacteriorhodopsin on the grid has an optical density of only ~0.0016 at 570 nm. However, the observed intensity changes correlate very well with the previous X-ray work. Koch *et al.* (1991) estimate 100% conversion to the M intermediate based on absorbance measurements of their multilayer samples. It follows that the intensity changes observed in their work can be used as a reference for estimating the extent of conversion into the M intermediate. From Table II, the extent of structural change observed by Koch *et al.* (1991) can be seen to be ~1.2 fold higher than the extent of conversion observed in the data set used in Figure 3c, implying that on average, our samples are ~80% converted to intermediates whose changes in diffraction intensity resemble those of the X-ray work. Assuming that M is the predominant intermediate under our experimental conditions, we conclude that the absolute extent of conversion to the M intermediate is ~80% in our case.

The above analysis also provides an explanation for the discrepancy between the earlier electron diffraction work and the later X-ray, neutron and electron diffraction experiments. All the latter experiments were carried out with bacteriorhodopsin samples that were fully hydrated, and therefore expected to undergo structural changes that would normally occur in the native cellular environment. The experiments carried out by Glaeser *et al.* (1986) used membranes embedded and dried in glucose and essentially devoid of water. The photocycle in glucose is probably different from the biologically relevant photocycle. There is also spectroscopic evidence that the photoreaction of bacteriorhodopsin in the dried state is different from its normal photocycle (Varo and Lanyi, 1990). Recent models of the photocycle have suggested the presence of two sequential M states (M1 and M2), with the main conformational change occurring between them (Varo and Lanyi, 1991). Thus, it is conceivable that the 'yellow' form trapped in the experiments of Glaeser *et al.* (1986) represents the M1 intermediate, and that the form studied in the present work represents the M2 intermediate.

Interpretation of structural change and implications for mechanism

During the latter half of the bacteriorhodopsin photocycle, a proton is taken up from the cytoplasm [see steps (iv) and (v) in Introduction]. An inspection of the structure of bacteriorhodopsin in the ground state reveals that the cytoplasmic half of the protein above the Schiff base is hydrophobic and rather tightly packed. Since a more hydrophilic environment is necessary for protons to move, this leads to the speculation that a 'widening' of the structure may be required to transport a proton from the cytoplasm into the protein. The changes that we observe indicate a movement of helix F away from the channel in the cytoplasmic half of the protein, and it is plausible that this movement contributes to the required 'widening' of the structure to permit proton uptake from the cytoplasm. These observations also fit well with linear dichroism measurements which show that retinal tilts a further 3° out of the plane upon isomerization (Schertler *et al.*, 1991; Otto and Heyn, 1991). Assuming the β-ionone ring of retinal as the pivot point, such a tilt would be expected to force the polyene chain of retinal into closer contact with the side chain of Trp182 in helix F. Trp182 is the principal residue in contact with the upper cytoplasmic surface of retinal and the isomerization could therefore induce a movement in helix F, possibly by pivoting about Pro186. From the size of the density peaks in Figure 3C, the extent of this proposed tilting would involve a movement of up to 2 Å at the cytoplasmic end of helix F.

The large positive peak observed on helix G is present in the difference maps obtained for both wild-type bacteriorhodopsin and the mutant. Since the positive peak is not accompanied by a unique negative peak, the simplest interpretation is that the cytoplasmic portion of helix G is more ordered in the M state than in the ground state. The last few residues at the C-terminal portion of helix G, including Arg227, may be involved in this change. Replacement of Arg227 with Gln is known to slow down the decay of the M intermediate (Stern and Khorana, 1989). Besides this common feature, there are also differences in the structural changes observed for the mutant (Figure 3c) and the wild-type photocycle (Figure 3e and f). It is possible that these merely reflect differences between the energetic aspects of structural changes in wild-type bacteriorhodopsin

and the mutant. A more likely explanation is that the changes are genuine differences resulting from the different compositions of photointermediates present in the two cases, with helices F and B participating, respectively, at the M and N intermediate steps of the photocycle.

Whatever the interpretation of the differences in the maps observed for the wild-type and the D96G mutants, they agree rather well with the X-ray experiments of Koch *et al.* (1991) and Nakasako *et al.* (1991), notwithstanding the lower resolution in the latter work. For example, the different distributions of peaks in Figure 3 panels c and e,f also occur in the data reported in the two different X-ray experiments: the M intermediate in the D96N mutant has its most prominent peak near helix F (Koch *et al.*, 1991) whereas the M intermediate in wild-type bacteriorhodopsin has this peak diminished and has a stronger feature near helix B (Nakasako *et al.*, 1991). The present work therefore reconciles and confirms the previous work, and considerably extends it both in resolution and in interpretation.

Conformational changes are essential for function in a wide variety of proteins. Analysis of the high resolution structures of different conformations of proteins such as insulin, citrate synthase and aspartate amino transferase clearly shows the importance of changes in the disposition of closely packed α-helices for conformational rearrangements (Chothia and Lesk, 1985; McPhalen *et al.*, 1992). The presence of seven membrane-spanning segments is also a common structural motif found in the superfamily of membrane proteins that includes the visual rhodopsins, neurotransmitter receptors and several peptide receptors. In contrast to bacteriorhodopsin, all of these receptors activate a heterotrimeric G-protein complex. Extensive biochemical studies with rhodopsin and the β-adrenergic receptor have suggested that the cytoplasmic loop attached to helix F is especially important for the G-protein activation. The light-induced structural changes observed here in the cytoplasmic half of helices F and G in bacteriorhodopsin raise the intriguing possibility that similar motions may underlie signal transduction in this family of G-protein coupled receptors.

Outlook for future research

The experiments presented here show that it is possible to trap and characterize the M intermediate in the photocycle of bacteriorhodopsin. We hope to collect diffraction patterns from tilted specimens and to construct a complete three-dimensional structure for the M intermediate. The approach used here also sets the stage for studying the structural changes accompanying the formation and decay of other intermediates generated upon light absorption. Finally, the experiments illustrate the strength of combining information from mutagenesis and spectroscopy with high resolution structural studies. Mutants such as the recently reported Leu93→Ala substitution, which results in a long-lived O intermediate (Subramaniam *et al.*, 1991) may prove valuable in further elucidation of the structural changes in the pathway of light transduction in bacteriorhodopsin.

Materials and methods

Preparation of large two-dimensional crystalline patches

Purple membranes were isolated from strains of *Halobacterium halobium* (sp. GRB) carrying the D96G mutation (Soppa and Oesterhelt, 1989). Purified membrane fragments were then fused in the presence of detergent as described previously (Baldwin and Henderson, 1984) to generate large patches ($\sim 5-10$ μm in diameter) that were suitable for the electron diffraction experiments.

Preparation of carbon-coated grids for electron diffraction

Carbon films of 150–250 Å thickness were evaporated on to a freshly cleaved mica surface. The carbon films were detached by flotation on a clean air–water interface, and carefully lowered on to electron microscope grids (mesh size 400) and dried at room temperature. Before application of the purple membrane suspension to the carbon-coated grids, they were glow discharged for 20–30 s in the presence of amyl amine at 10^{-2} torr. Freshly glow-discharged grids displayed a high affinity for the purple membranes. The resulting strong interaction of the membranes with the amyl amine-treated carbon surface led to disorder in the crystal and consequently to poor diffraction patterns. However, pre-wetting of the grids with 1% octyl glucoside following the glow discharge greatly enhanced the quality of the diffraction patterns obtained, while still allowing enough membranes to be attached to the film. Presumably, this was caused by the presence of a mixed surface film of amyl amine and octyl glucoside on the grid. This procedure was therefore used for most of the experiments.

Preparation of specimens for electron diffraction

We have assembled a plunge-freeze apparatus to trap intermediates generated upon illumination of two-dimensional crystals of bacteriorhodopsin (schematic shown in Figure 2). The heart of the apparatus is a 'controlled environment vitrification system' designed and constructed by Dr Y.Talmon and colleagues (Bellare *et al.*, 1988) which permits preparation of specimens for cryoelectron microscopy under conditions of controlled temperature and humidity. The main features of the apparatus are a specially constructed chamber, in which the relative humidity can be maintained at >95%, and a spring-loaded steel plunger, to which a pair of forceps is clamped. Release of the plunger triggers opening of a door in the bottom face of the chamber, through which the plunger is propelled at a speed of 2 m/s. In a typical experiment, 4–5 μl of a suspension of fused purple membranes (concentration 1–3 mg/ml, pH 5.5, 7.0 or 8.5) was applied to an electron microscope grid prepared as described above. After incubation inside the chamber for a period of 10–15 s, excess liquid was manually blotted away with filter paper. The grid, which retained a thin film of liquid and a small number of adsorbed crystals, was then plunged into liquid ethane and immediately transferred to liquid nitrogen. The cooling rate under the conditions of our experiment is expected to be >100 000°C/s (Dubochet *et al.*, 1988). Hence the sample temperature should drop below 0°C within 300 μs of its contact with liquid ethane. All subsequent handling of the specimen, including cryotransfer and electron diffraction, was carried out at liquid nitrogen temperatures.

To prepare a specimen frozen in the ground state, a grid with attached crystals was light-adapted with green illumination (wavelength 550–570 nm) and the rest of the experiment was carried out in a darkened laboratory. To prepare a specimen trapped in the M state, a grid was illuminated with green light from a photodiode-xenon flash lamp assembly (same wavelength as above) 10 or 20 ms prior to contact with liquid ethane. Under the conditions of our experiment, these times are accurate to within ±2 ms. The silicon photodiode was mounted outside the chamber and positioned to detect the arrival of the grid at a predetermined height above the surface of the liquid ethane. The change in the output of the diode was used to trigger a xenon flash lamp (pulse-width ~600 μs, energy output ~0.5 J/pulse) whose beam intersected the path of the falling grid. The relative height of the diode with respect to the falling grid was easily adjustable, thus allowing precise alignment of the light beam on to the grid. To verify that the light from the flash lamp had indeed illuminated the entire grid, a Polaroid photograph of the descending plunger was taken for every grid. The direction of illumination was approximately perpendicular to the surface of the grid, and is therefore optimal for excitation of the retinylidene chromophores, which are distributed parallel to the plane of the grid.

Recording and processing of electron diffraction patterns

Electron diffraction patterns were recorded on Kodak SO-163 film using a Philips CM-12 microscope operating at 120 kV using a 25 μm C2 aperture and a highly excited C1 lens. The microscope was equipped with a GATAN cryotransfer system, cold stage and cryo-blades to prevent frost accumulation on the specimens. Typically, exposure times of 7.5–10 s were used in conjunction with a camera length of ~1.0 m and a beam diameter of 2–2.5 μm on the grid. This corresponded to a dose of 2–5 electrons/Å^2. Larger doses resulted in an increase in the noise level of the difference Fourier maps (data not shown), an effect that is most probably caused by variations in the nature of electron beam damage to the crystal. Digitization of the diffraction patterns, measurement of background-corrected spot intensities and refinement of twin proportions, scale and temperature factors, crystal

tilt axes and tilt angles were carried out as described by Baldwin and Henderson (1984) with the modifications described by Ceska and Henderson (1990). Calculation of difference Fourier maps used phases from Henderson *et al.* (1990) with 143 coefficients in projection (Figure 3) and 715 in the limited resolution 3D map (Figure 4).

Some tests were carried out to measure the lack of flatness of the crystals, a potential cause of increased noise levels. The lack of flatness was found to vary from 1 to 7° in different crystals. However, the effect of correcting for this lack of flatness on the quality of the difference maps was much smaller than the effect of doubling the electron dose. Thus, the lack of flatness of the adsorbed crystals does not appear to limit the quality of the maps at present. This may, however, be of greater importance in the processing of diffraction patterns obtained from highly tilted specimens.

Calculation of correlation coefficients

Comparisons of electron diffraction amplitudes were carried out using individual measurements of ΔF, the amplitude changes for individual (h,k) reflections. Comparisons between X-ray diffraction intensity changes and electron diffraction intensity changes were carried out using measurements of ΔI, the intensity change for either overlapping or non-overlapping reflections. Correlation coefficients and relative extents of structural changes between pairs of data sets were calculated as follows:

Correlation coefficient =

$$\frac{\Sigma\Delta F_1 * \Delta F_2}{\sqrt{\Sigma\Delta F_1^2 * \Sigma\Delta F_2^2}} \quad \text{or} \quad \frac{\Sigma\Delta I_1 * \Sigma I_2}{\sqrt{\Sigma\Delta I_1^2 * \Sigma\Delta I_2^2}}$$

Extent of change =

$$\frac{\Sigma W_F \dfrac{\Delta F_2}{F_2}\Big/\dfrac{\Delta F_1}{F_1}}{\Sigma W_F} \quad \text{or} \quad \frac{\Sigma W_I \dfrac{\Delta I_2}{I_2}\Big/\dfrac{\Delta I_1}{I_1}}{\Sigma W_I}$$

summed over all reflections in which both measurements or ΔF/F are $>0.6\sigma$ where W_F =

$$\frac{1.0}{\left[\dfrac{\sigma^2_{\Delta F_1/F_1}}{\left(\dfrac{\Delta F_1}{F_1}\right)^2} + \dfrac{\sigma^2_{\Delta F_2/F_2}}{\left(\dfrac{\Delta F_2}{F_2}\right)^2}\right]} \sqrt{\left|\frac{\dfrac{\Delta F_1}{F_1}}{\dfrac{\Delta F_2}{F_2}}\right|}$$

and $\sigma^2_{\Delta F_1/F_1}$ and $\sigma^2_{\Delta F_2/F_2}$ are the variances in experimental measurements of $\Delta F_1/F_1$ and $\Delta F_2/F_2$. A similar expression was used for W_I.

By definition, the correlation coefficient of a given data set with itself is 1.00. Large positive correlation coefficients indicate that similar structural changes occur in the data sets that are being compared. A zero correlation coefficient indicates that the nature of protein structural changes in the two data sets that are being compared is completely uncorrelated, while a negative coefficient indicates would mean opposite changes in structure. Thus in Table I, from the calculated correlation coefficients of 0.87 and 0.66 for crystals D290 and F333 with the averaged data set used for Figure 3c, we conclude that (i) light-induced structural changes in both crystals are similar to the averaged structural change shown in Figure 3c and (ii) the structural change observed in crystal D290 (D96G mutant) is closer to the average than the change observed in crystal F333 (wild-type), which is to be expected since the data in Figure 3c were obtained from the mutant.

Acknowledgements

We thank Joyce Baldwin, Gebhard Schertler and Jorg Tittor for helpful discussions, Jens Riesle for assistance with the construction and expression of the D96G mutant and the Royal Society, London and the Herchel-Smith Foundation for the award of fellowships to S.S. and M.G. respectively. Finally, we thank Ishi Talmon and the workshop at Technion-Israel Institute of Technology for supplying the Controlled Environment Vitrification System and Nigel Unwin for the gift of the xenon lamp.

References

Baldwin,J. and Henderson,R. (1984) *Ultramicroscopy*, **14**, 319–336.
Bellare,J., Davis,H.T., Scriven,L.E. and Talmon,Y. (1988) *J. Electron Microsc. Techn.*, **10**, 87–111.
Ceska,T.A. and Henderson,R. (1990) *J. Mol. Biol.*, **213**, 539–560.
Chothia,C. and Lesk,A.M. (1985) *Trends Biochem. Sci.*, **14**, 116–118.
Dencher,N.A., Dresselhaus,D., Zaccai,G. and Buldt,G. (1989) *Proc. Natl. Acad. Sci. USA*, **86**, 7876–7879.
Dubochet,J., Adrian,M., Chang,J.J., Homo,J.C., Lepault,J., McDowell,A.W. and Schultz,P. (1988) *Q. Rev. Biophys.*, **21**, 129–228.
Frankel,R.D. and Forsyth,J.M. (1985) *Biophys. J.*, **47**, 387–393.
Glaeser,R.M., Baldwin,J.M., Ceska,T.A. and Henderson,R. (1986) *Biophys. J.*, **50**, 913–920.
Henderson,R., Baldwin,J.M., Ceska,T., Zemlin,F., Beckmann,E. and Downing,K.H. (1990) *J. Mol. Biol.*, **213**, 899–929.
Khorana,H.G. (1988) *J. Biol. Chem.*, **263**, 7439–7442.
Koch,M.H.J., Dencher,N.A., Oesterhelt,D., Plohn,H.-J, Rapp,G. and Buldt,G. (1991) *EMBO J.*, **10**, 521–526.
Lozier,R.H., Bogomolni,R.A. and Stoeckenius,W. (1975) *Biophys. J.*, **15**, 955–962.
Marinetti,T., Subramaniam,S., Mogi,T., Marti,T. and Khorana,H.G. (1989) *Proc. Natl. Acad. Sci. USA*, **86**, 529–533.
McPhalen,C., Vincent,M.G., Picot,D., Jansonius,J.N., Lesk,A.M. and Chothia,C. (1992) *J. Mol. Biol.*, **227**, 197–213.
Nakasako,M., Kataoka,M., Amemiya,Y. and Tokunaga,F. (1991) *FEBS Lett.*, **292**, 73–75.
Oesterhelt,D., Brauchle,C. and Hampp,N. (1991) *Q. Rev. Biophys.*, **24**, 425–478.
Otto,H. and Heyn,M.P. (1991) *FEBS Lett.*, **293**, 111–114.
Otto,H., Marti,T., Holz,M., Mogi,T., Stern,L.J., Engel,F., Khorana,H.G. and Heyn,M. (1990) *Proc. Natl. Acad. Sci. USA*, **87**, 1018–1022.
Schertler,G.F.X., Lozier,R., Michel,H. and Oesterhelt,D. (1991) *EMBO J.*, **10**, 2353–2361.
Soppa,J. and Oesterhelt,D. (1989) *J. Biol. Chem.*, **264**, 13043–13048.
Stern,L.J. and Khorana,H.G. (1989) *J. Biol. Chem.*, **264**, 14202–14208.
Stoeckenius,W., Lozier,R.H. and Bogomolni,R.A. (1979) *Biochim. Biophys. Acta*, **505**, 215–278.
Subramaniam,S., Greenhalgh,D.A., Rath,P., Rothschild,K.J. and Khorana,H.G. (1991) *Proc. Natl. Acad. Sci. USA*, **87**, 6873–6877.
Tittor,J., Soell,C., Oesterhelt,D., Butt,H. and Bamberg,E. (1989) *EMBO J.*, **8**, 3477–3482.
Varo,G. and Lanyi,J.K. (1990) *Biophys. J.*, **59**, 313–322.
Varo,G. and Lanyi,J.K. (1991) *Biochemistry*, **30**, 5016–5022.

Received on August 20, 1992; revised on October 2, 1992